Journal of Computational Physics 228 (2009) 6796–6810

Contents lists available at ScienceDirect

Journal of Computational Physics

journal homepage: www.elsevier.com/locate/jcp

A 1D–3D mixed method for the numerical simulation of blast waves in confined geometries

Adel M. Benselama *, Mame J.-P. William-Louis, François Monnoyer

Univ Lille Nord de France, F-59000 Lille, France
UVHC, LME, F-59313 Valenciennes, France

ARTICLE INFO

Article history:
Received 13 February 2009
Received in revised form 28 May 2009
Accepted 5 June 2009
Available online 25 June 2009

PACS:
47.40.Rs

Keywords:
Blast waves
Remapping techniques
Cartesian mesh
Confined domains

ABSTRACT

Blast wave generated by a high detonating spherical charge and propagating in confined domains is modeled using the Euler equations. The problem is split into two parts. The first calculation part relies on spherical isotropy to solve the problem in the radial component. Overpressure distribution is presented and shows a very good agreement with experimental and numerical data. The one-dimensional data need to be made three-dimensional mesh-compatible thanks to an appropriate remapping technique. To this end, a remapping technique is presented and its effectiveness, accuracy and efficiency are demonstrated. The second calculation part consists of a three-dimensional computation fed with the remapped data. The effectiveness of this mixed approach is demonstrated through three-dimensional applications in confined domains.

1. Introduction

The increasing proportion of covered ways and tunnels in urban and suburban areas, together with the denser rail and road traffic, represent a stronger risk of severe accidents due to hazardous materials. As confinement is an aggravation factor of explosion effects, special safety measures have to be met in crowded underground structures and analysis tools are needed to simulate critical scenarios. This requires a better knowledge of blast waves in confined areas.

Conceptually, the main characteristic for any explosion is the rapid release of a huge quantity of energy from a compact volume in a very short time, typically of the order of the microsecond, which provokes a local pressure increase. A supersonic wave is subsequently generated and propagates away from the detonation origin. Explosion sources may be solid detonating materials, flammable gas–air mixtures at appropriate proportions or even confined vapor or gas phase. For almost all cases, highly exothermic chemical reactions happen. Usually, the criterion for certain level of damage is the maximal overpressure predicted to be produced at a given distance from the explosion origin [1,2].

High explosive detonation and the generated blast wave have been extensively studied both theoretically and experimentally since several decades [2,3]. The development of numerical – and engineering simulation commercial – tools, such as DYNA3D, CFX and AUTO-DYN, dedicated to such applications has turned to a reality, but so far need considerable computer resources to make realistic simulations [4–6]. This may be explained by the use of the three-dimensional computation from the very blast onset where, from stiffness considerations of the problem, extremely small time steps are required.

* Corresponding author. Address: UVHC, LME, F-59313 Valenciennes, France. Tel.: +33 327511971; fax: +33 327511961.
E-mail address: MustaphaAdel.Benselama@univ-valenciennes.fr (A.M. Benselama).

0021-9991/$ - see front matter © 2009 Elsevier Inc. All rights reserved.
doi:10.1016/j.jcp.2009.06.010

Nomenclature

Greek letters

γ	heat capacity ratio for perfect gas
λ	mesh numerical frequency, $\lambda = M_c^{1/3}/\Delta x^{3D}$ ($kg^{1/3}/m$)
ω	constant for Jones–Wilkins–Lee (JWL) equation of state
ρ	density (kg/m^3)
Σ	three-dimensional mesh cell surface area (m^2)

Latin letters

$\mathbf{u}$	velocity vector
a	speed of sound (m/s)
A, B, C, R_1, R_2	constants for the JWL equation of state
E	total specific internal energy, $E = e + \frac{1}{2}(u^2 + v^2 + w^2)$ (J/kg)
e	specific internal energy (J/kg)
F, G, K	flux vectors
H	total specific enthalpy, $H = E + \frac{p}{\rho}$ (J/kg)
L	one-dimensional domain radius (m)
M	mass (kg)
p	pressure (Pa)
R	radius (m)
r	radial coordinate (m)
S	vector of source terms
T	total simulation time (s)
t	time (s)
U	vector of conservative variables
u, v, w	velocity components (m/s)
V	three-dimensional mesh cell volume (m^3)

Indices

c	explosive charge
EOS	equation of state
h	enthalpy
r	radial component
ref	reference conditions

In the literature two main approaches exist to simulate the detonation and the subsequent traveling blast wave. The simplest and perhaps the most intuitive one is the energy source term model. Condensed explosives do explode at constant rate so much so that their detonation velocity is constant [3]. This means that released energy per time unit remains constant during the whole detonation process. For this reason, it would be a good approximation to consider the detonation as a homogeneous process that occurs inside the explosive charge. The explosive charge will then be considered as an energy source, located in a finite domain, and determined by the specific energy, the detonation velocity and the mass of the considered explosive. The second approach is the balloon analogue that assumes the explosive charge materials have been transformed, at constant volume, into hot gases at the so-called Chapman–Jouguet state [3,7]. Since this approach assumes the transformation finished, it does not enable to simulate the detonation process itself. Nevertheless, all thermodynamic parameters, including the pressure and the density, are known at this final equilibrium state. The solution process must then start with the onset of the blast wave.

Even if the blast wave propagation has in general three-dimensional patterns it is possible to consider, at the onset of the explosion, the wave freely and isotropically traveling. This spherical one-dimensional approach has proven to be valid as long as the blast wave propagates in resting free domain [1,3]. In this case, it represents a good alternative to fully three-dimensional approaches that are necessarily much more computer resources consuming.

The present work combines the one- and three-dimensional approaches in an efficient way. Starting after the detonation, the one-dimensional model is used as far as applicable. The simulation then proceeds with a three-dimensional model. The initial conditions are provided by the remapping technique, which transfers the one-dimensional data onto the three-dimensional mesh.

In this paper, the one-dimensional approach using the balloon analogue is applied to well documented test cases and compared to experimental and numerical data [1,8,9]. After discussing the remapping technique, the 1D–3D combined method is applied to closed three-dimensional geometries and their interactions with the propagation of the blast wave are presented.

2. The one-dimensional spherical model

2.1. Physical and numerical models

Detonation, which precedes the blast wave, is modeled by the balloon analogue [7]. Flow conditions for statically pressurised gases are specified within a balloon occupying the volume of the explosive charge and separated from the atmosphere by a fictitious membrane. The pressure is set to the detonation pressure, or the so-called Chapman–Jouguet pressure (see Table 1), and the specific internal energy to the energy of the charge e_c. The fictitious balloon membrane plays the role of the diaphragm as in a shock tube. Its burst produces an expanding blast wave traveling outwards with an inward rarefaction counterpart.

The hypothesis of spherical symmetry explosion is a good assumption since, either in an infinite region or before obstacles intercept the front wave pressure, an initially spherical detonating and blasting explosive charge isotropically propagates [1,3,10]. In this case, the one-dimensional spherical equations can be used with a good level of confidence to describe the problem. Fig. 1 depicts the domain where the numerical problem is solved. The one-dimensional computational domain $[0, L]$ is divided into two sub-domains. The first one, where $0 \leqslant r \leqslant R_c$, is the explosive charge domain. The second sub-domain, where $R_c \leqslant r \leqslant L$, is the ambient atmosphere region encompassing the charge.

2.1.1. Governing equations

The dynamic and thermal behavior of propagation phenomena is governed by the unsteady transport equations for mass, momentum an energy. Viscous and thermal diffusion processes may play a significant role in the overall transport phenomena but they are not included in the form of classical diffusion terms leading to the Navier–Stokes equations, as this would require very fine spatial discretizations in the regions of strong velocity and temperature gradients. The corresponding grid scales would be extremely small and would involve mesh size beyond the capacity of the current computers. Consequently, thermal and viscous diffusion effects can be implemented – if needed – as global source terms added to the Euler transport equations, which read considering the radial symmetry as follows:

$$\frac{\partial U}{\partial t} + \frac{\partial (F)}{\partial r} = S, \quad (r, t) \in [0, L] \times [0, T], \tag{1}$$

where U is the conservative variables vector, F the radial flux vector and S the source terms vector, defined by:

$$U = \begin{pmatrix} \rho \\ \rho u_r \\ \rho E_r \end{pmatrix}, \quad F = \begin{pmatrix} \rho u_r \\ \rho u_r^2 + p \\ (\rho E_r + p) u_r \end{pmatrix}, \quad \text{and } S = \begin{pmatrix} -\frac{2}{r}\rho u_r + S_\rho \\ -\frac{2}{r}\rho u_r^2 + S_{\rho u_r} \\ \left(-\frac{2}{r}(\rho E_r + p) u_r + S_{\rho E_r}\right) \end{pmatrix}. \tag{2}$$

$S_\rho, S_{\rho u_r}$ and $S_{\rho E_r}$ are possible mass, kinetic and energy source terms, respectively, and may include diffusion effects. However, in the case of blast wave propagation, these terms may be neglected compared to the convective terms.

The system of Eq. (1) is complemented by equations of state and suitable initial and boundary conditions.

In the literature, a variety of laws of state are suggested to describe the detonation products [11–13]. The simplest equation of state proposed is the perfect gas law. For calorically perfect gases, it reads:

$$p = (\gamma - 1)\rho e, \tag{3}$$

and the corresponding expression of the speed of sound is:

$$a = \sqrt{\gamma \frac{p}{\rho}}. \tag{4}$$

Table 1
Parameters values used for JWL law describing T.N.T. explosive.

Specific energy, e_c kJ/kg	Density, ρ_c $10^3 \times$ kg/m^3	Detonation speed, u_c km/s	Detonation pressure, p_{CJ} GPa	A 10^{11} Pa	B 10^9 Pa	C 10^{14} Pa	R_1 –	R_2 –	ω –
4870	1.58	8.50	21	3.73	3.74	7.34	4.15	0.90	0.35

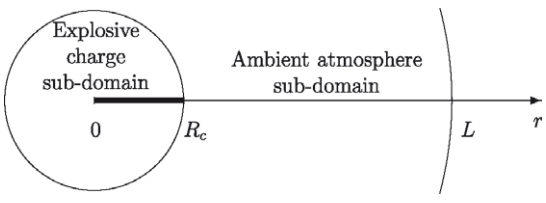

Fig. 1. Domains involved in the one-dimensional model.

More specific and sophisticated laws for hot detonation products are also suggested. Because of its simplicity and exhaustiveness, *vis-a-vis* a large variety of explosives, the most commonly used is the Jones–Wilkins–Lee (JWL) law [14,15]:

$$p = A\left(1 - \frac{\omega}{R_1}\frac{\rho}{\rho_c}\right)\exp(-R_1\rho_c/\rho) + B\left(1 - \frac{\omega}{R_2}\frac{\rho}{\rho_c}\right)\exp(-R_2\rho_c/\rho) + \omega\rho e, \tag{5}$$

with the speed of sound accordingly defined by:

$$a = \left(AR_1\frac{\rho_c}{\rho^2}\exp\left(-R_1\frac{\rho_c}{\rho}\right) + BR_2\frac{\rho_c}{\rho^2}\exp\left(-R_2\frac{\rho_c}{\rho}\right) + C\frac{\omega+1}{\rho_c}\left(\frac{\rho}{\rho_c}\right)^{\omega}\right)^{\frac{1}{2}}. \tag{6}$$

For TNT-like explosive, the constants involved in this equation are tabulated in Table 1.

Outside of the explosive region, the surrounding atmosphere is supposed obeying the perfect gas law (3).

The boundary conditions applied to Eq. (1) are:

- a symmetry condition at the explosive charge center, $r = 0$, that is:

$$\begin{cases} \left(\frac{\partial\rho}{\partial r}\right)_{r=0} = 0 \\ u_r(r=0) = 0 \\ \left(\frac{\partial(\rho E_r)}{\partial r}\right)_{r=0} = 0 \end{cases} \tag{7}$$

- a non-reflective condition at the outer boundary, $r = L$, that is:

$$\begin{cases} \left(\frac{\partial\rho}{\partial r}\right)_{r=L} = 0 \\ \left(\frac{\partial(\rho u_r)}{\partial r}\right)_{r=L} = 0 \\ \left(\frac{\partial(\rho E_r)}{\partial r}\right)_{r=L} = 0 \end{cases} \tag{8}$$

In compatibility with the balloon analogue model, the initial conditions read:

- for $0 \leqslant r < R_c, \rho = \rho_c, u_r = 0$ and $p = p_{EOS}(e_c, \rho_c)$;
- for $R_c \leqslant r < L, \rho = \rho_{ref}, u_r = 0$ and $p = p_{ref}$.

p_{EOS} is given even by (3) if the detonation products are supposed to obeying perfect gas law, or by (5) if they are supposed to obeying JWL law.

2.1.2. Implementation and numerical issues

The finite-difference scheme S^{α}_{β} is used in the present one-dimensional study [16]. It is a second-order accurate in space and explicit two-step time scheme. The solution proceeds on the whole spatial domain from the known step n to the new step $(n+1)$ by the two-step procedure:

- the predictor step:

$$\widetilde{U}_i = (1-\beta)U_i^n + \beta U_{i+1}^n - \alpha\frac{\Delta t}{\Delta r}(F_{i+1}^n - F_i^n) + \Delta t\alpha S_i, \tag{9}$$

- the corrector step:

$$U_i^{n+1} = U_i^n - \frac{\Delta t}{2\alpha\Delta r}\left[(\alpha-\beta)F_{i+1}^n + (2\beta-1)F_i^n + (1-\alpha-\beta)F_{i-1}^n + \widetilde{F}_i - \widetilde{F}_{i-1}\right] + \frac{\Delta t}{2\alpha}S_i, \tag{10}$$

where $\widetilde{F}_i \equiv F(\widetilde{U}_i)$ and $\alpha \neq 0$. Δr and Δt are the space and time steps, respectively. Subscript i is associated to the space coordinate r. α and β are set to 1/2, which corresponds to the two-step version of the Lax–Wendroff scheme.

In addition, the stability criterion of this problem is the classical CFL condition given by:

$$\Delta t = CFL \times \min\left(\frac{\Delta r}{(|u_r| + a)}\right). \tag{11}$$

$CFL = 0.8$ was found to be sufficient for all performed simulations. Because strong gradients are involved during the computations, some numerical oscillations may occur and are prevented by using a Flux-Corrected Transport algorithm proposed by Boris et al. [17].

2.2. Results

The first test case is the detonation of an 0.635 g TNT explosive charge. In the early stage of the simulation, the very high speed of sound due to prevailing hot gases leads to very small allowable time steps, of the order of 10^{-11} s. Pressure and temperature decay in time and the time step consequently increases up to about 10^{-9} s. Using perfect gas law to describe the hot gases state reduces the time step, of two orders of magnitude, compared to simulations using JWL law. Fig. 2 presents the evolution of the peak of the overpressure Δp ($\Delta p = p - p_{ref}$, where p_{ref} is the ambient pressure) versus the distance from the center of the explosive charge represented by a reduced distance $Z = r/M_c^{1/3}$. M_c is the mass of the explosive charge. The calculations with JWL or perfect gas equation of state give results which are in very good agreement with the experimental data of Mills [8] and Henrych [9] as well as with Brode's calculations [1]. Nevertheless, the assumption of perfect gas to describe the hot products of the detonation slightly overestimates the maximum overpressure specially in the charge domain. This fact may easily be understood since the perfect gas model neglects the attractive forces between the gas molecules. This assumption is correct to describe weakly dense gas but misestimates the real behavior of more dense gases where a pressure exceed must be considered to overbalance the attractive Van Der Waals force at a given temperature.

The use of the JWL and the perfect gas models is illustrated in Figs. 3–5 where the distribution of the calculated relative overpressure, the radial velocity and the density, respectively, is represented at different times.

At the beginning of the detonation, a shock wave propagates out from the hot gases/air interface. This shock decays as it travels away from the blast center due to the considered sphericity pattern of the propagating phenomena. Because of

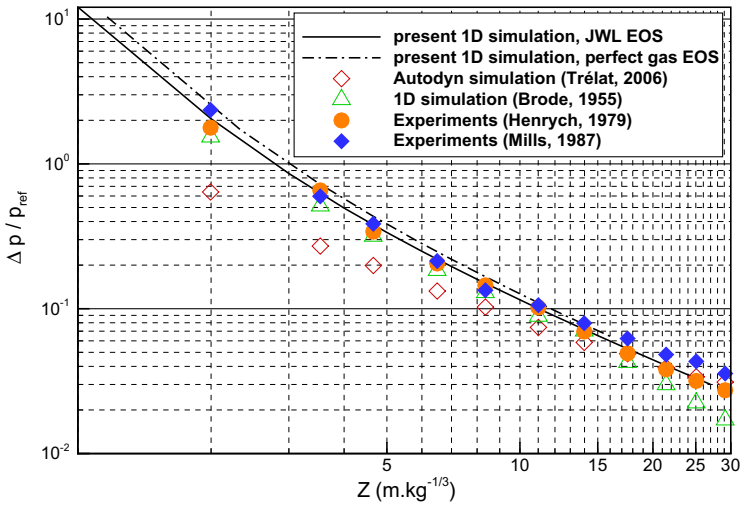

Fig. 2. Radial distribution of the overpressure maximum peak.

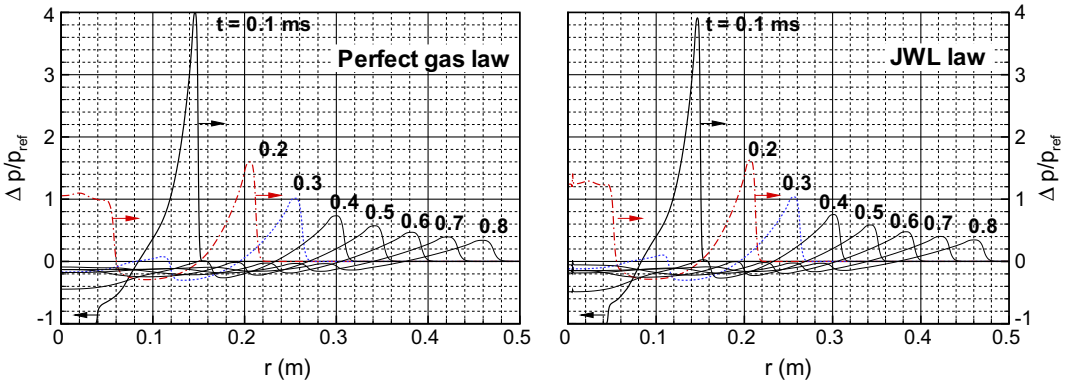

(a) Perfect gas law. (b) JWL law.

Fig. 3. Distribution of the relative overpressure.

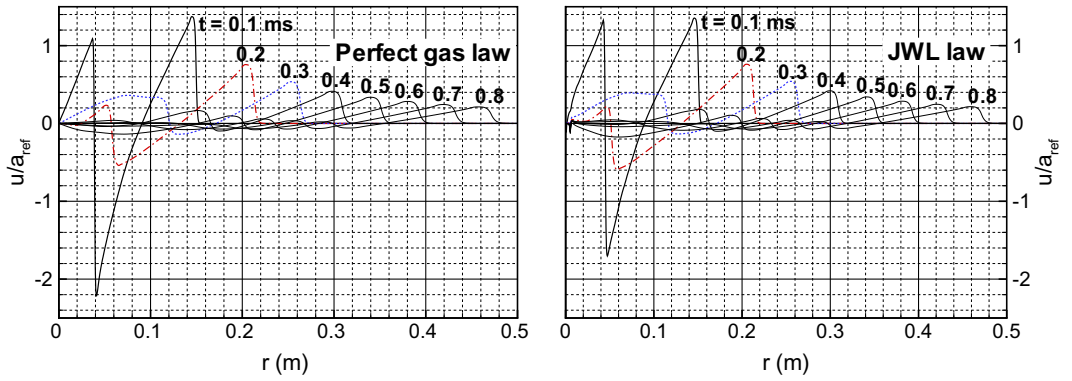

(a) Perfect gas law. (b) JWL law.

Fig. 4. Distribution of the non-dimensional radial velocity.

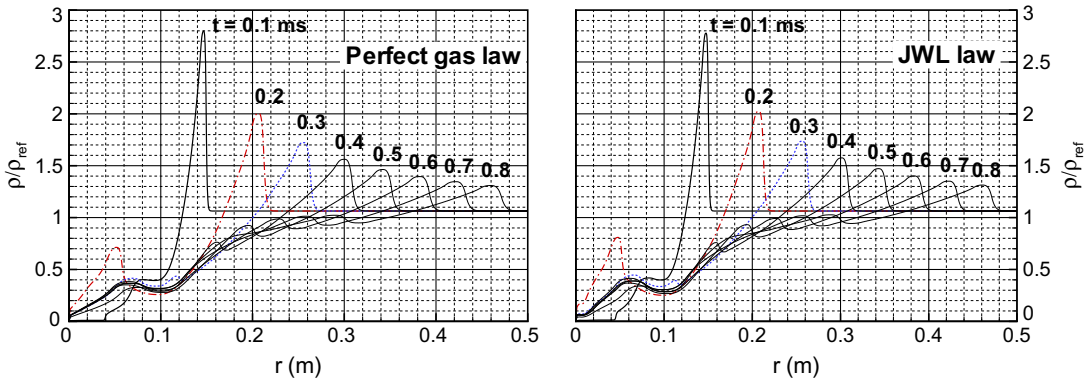

(a) Perfect gas law. (b) JWL law.

Fig. 5. Distribution of the non-dimensional density.

the rapid expansion of the fluid, a rarefaction happens at the blast charge volume followed by an inbound compression wave propagating from the contact surface. In a equivalent manner to the outbound wave, the overpressure of this inbound propagating compression wave increases as it approaches the blast center. When it reaches the blast center, and due to the proper symmetry of this point, this wave is reflected back and at this time propagates outward until it catches up the contact surface. One part of this wave continues propagating outward, while the other is reflected back leading to a series of successive decaying outbound compression waves. In the region upstream of the contact surface, the perfect gas assumption leads to underestimating the overpressure and overestimating the speed of sound compared to the JWL law. For the region downstream of the contact surface, the perfect gas assumption leads to overestimating the overpressure while the velocity and density are almost identical using either laws. So this leads to overestimating the speed of sound and badly estimating the arrival times of the compression waves, other than the primary shock wave, when using the perfect gas law.

3. The three-dimensional model

3.1. Governing equations

The general formulation of conservative Euler equations for compressible fluid reads:

$$\frac{\partial U}{\partial t}+\frac{\partial F(U)}{\partial x}+\frac{\partial G(U)}{\partial y}+\frac{\partial K(U)}{\partial z}=S, \tag{12}$$

where U is the variables vector, and $F(U), G(U)$ and $K(U)$ are the fluxes in x, y and z directions, respectively. They are defined by:

$$U = \begin{pmatrix} \rho \\ \rho u \\ \rho v \\ \rho w \\ \rho E \end{pmatrix}, \quad F(U) = \begin{pmatrix} \rho u \\ \rho u^2 + p \\ \rho uv \\ \rho uw \\ \rho u(E + p/\rho) \end{pmatrix}, \tag{13}$$

$$G(U) = \begin{pmatrix} \rho v \\ \rho uv \\ \rho v^2 + p \\ \rho vw \\ \rho v(E + p/\rho) \end{pmatrix}, \quad K(U) = \begin{pmatrix} \rho w \\ \rho uw \\ \rho vw \\ \rho w^2 + p \\ \rho w(E + p/\rho) \end{pmatrix}. \tag{14}$$

S is the source term vector that may include the viscous and thermal diffusion energy terms:

$$S = (S_\rho, S_{\rho u}, S_{\rho v}, S_{\rho w}, S_{\rho E})^T. \tag{15}$$

$S_\rho, S_{\rho u}, S_{\rho v}, S_{\rho w}, S_{\rho E}$ are mass, x-, y-, z-momentum and energy source terms, respectively, that may include dissipative terms. Like the one-dimensional case, the viscous and thermal terms are supposed negligible compared to the convective terms in the present calculations. Eq. (12) is completed by boundary and initial conditions. For walls, slip conditions are applied while for far field, non-reflective boundaries conditions are used.

3.2. Numerical issues

The unsteady Euler three-dimensional problem (12) is solved by an in-house developed software [18]. The numerical method is a unstructured finite-volume cell-centered approach using the classical upwind scheme and a two-stage explicit discretization in time, yielding a second-order accuracy in both space and time. In order to prevent numerical oscillations, which may occur in regions with strong gradients, the total variation diminishing (TVD) minmod scheme is used [20]. The spatial discretization is performed with an automatic Cartesian grid generator [19]. In addition, the CFL condition has to be satisfied in order to guarantee the stability of the numerical scheme. To construct the CFL for the three-dimensional case, space step is defined by the ratio of the cell volume V to the half of its surface area Σ, i.e.:

$$\Delta t = CFL \times \min\left(\frac{\Delta x^{3D}}{(\|\mathbf{u}\| + a)}\right), \quad \Delta x^{3D} = \frac{2V}{\Sigma}. \tag{16}$$

The value of $CFL = 0.8$ was found to be suitable to ensure the stability of the computational scheme for all tested cases.

The flow is supposed to be initially at rest over the three-dimensional domain except inside the sphere of radius L encompassing the explosive charge where the flow is disturbed by the blast wave calculated by the one-dimensional procedure and made three-dimensional mesh-compatible thanks to the 1D–3D remapping algorithm described in the following.

3.3. Data remapping methods and results

The issue is to remap data from a one-dimensional mesh onto a less finer three-dimensional Cartesian cell i at a given time t_0. The relative three-dimensional mesh coarseness is dictated by the fact that if a small one-dimensional mesh size is computationally affordable, a three-dimensional mesh with equivalent size is not. For remapping data an appropriate technique must be developed that satisfies the criteria of: (i) robustness, i.e. as less sensitive to the mesh size variations as possible, (ii) accuracy and, (iii) as less as possible computer resources consuming. Some algorithms were tested and among them two are presented here.

The first technique is remapping in time by taking the time variations of the quantity to remap integrated over a specific three-dimensional time step Δt^{3D}. Since the specific three-dimensional space step is larger than the one-dimensional one, Δt^{3D} is effectively larger than Δt^{1D} at constant CFL. For explanatory purpose, it is supposed to remap the pressure p from a one-dimensional onto a three-dimensional stencil, other physical quantities are dealt with in the same fashion. At the three-dimensional cell i, the time variations of p_i^{3D} integrated over a three-dimensional time step Δt^{3D} reads:

$$p_i^{3D}(t_0) = p_i^*(t_0 - \Delta t^{3D}) + \int_{t_0 - \Delta t^{3D}}^{t_0} \left(\frac{\partial p^{1D}}{\partial t}\right)_i^* (t) dt, \tag{17}$$

where p_i^* and $(\partial p^{1D}/\partial t)_i^*$ are linear interpolations, at the cell i center, of the pressure and its time derivative at the current time.

The second technique is space remapping by taking the chord mean value of the quantity to remap. The cell pressure $p_i^{3D}(t_0)$ is given by the expression:

$$p_i^{3D}(t_0) = \frac{\int_{r_M}^{r_N} p^{1D}(r, t_0) dr}{r_N - r_M} \tag{18}$$

where M and N are the intersection points between the i cell surface and the line that joins its center Q to the charge center C as illustrated by Fig. 6.

In order to study the behavior of each remapping technique, the mesh size is represented by the corresponding numerical wave frequency $\lambda = \frac{M_c^{1/3}}{\Delta x^{3D}}$ as suggested by [7]. The Fig. 7 represents the overpressure distribution calculated by the one-dimensional approach compared to the overpressure in the three-dimensional domain obtained after applying the remapping procedure. The remapping procedure is applied to the solution at 45 μs after the blast onset of 0.3 kg of TNT. Two numerical wave frequencies are used, namely $\lambda = 57$ for Fig. 7(a) and (b) and $\lambda = 114$ for Fig. 7(c) and (d). The time integral and the chord mean value techniques are accurate, where the local error is less than 5%, provided that the mesh is sufficiently refined, i.e. for $\lambda = 114$.

This is corroborated by Fig. 8 that represents the mesh sensitivity of the mean chord value and time integral techniques to capture key overpressures at different numerical wave frequencies. The considered overpressures are those of the inbound and outbound waves. For low frequencies, when $\lambda < 100$, both techniques capture the overpressures given by the

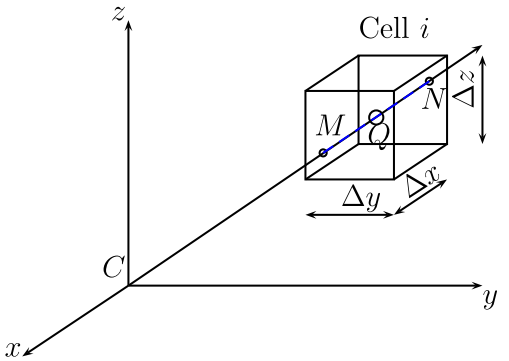

Fig. 6. Mean value calculated over the chord (MN).

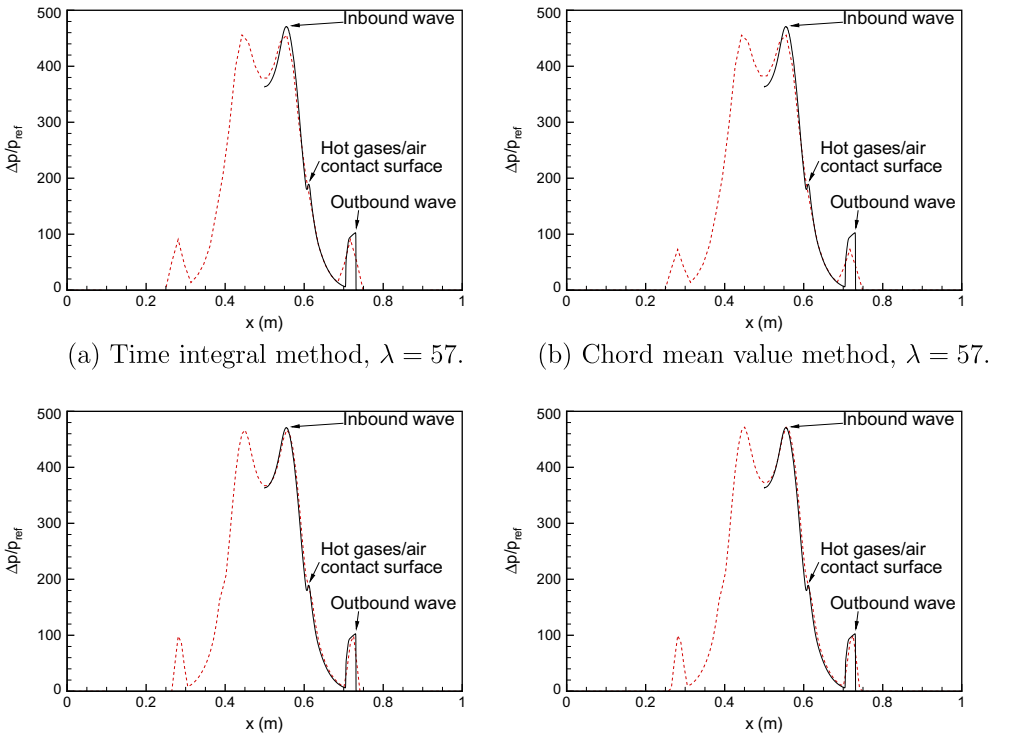

Fig. 7. Pressure distribution (–, one-dimensional solution, – – three-dimensional remapped data).

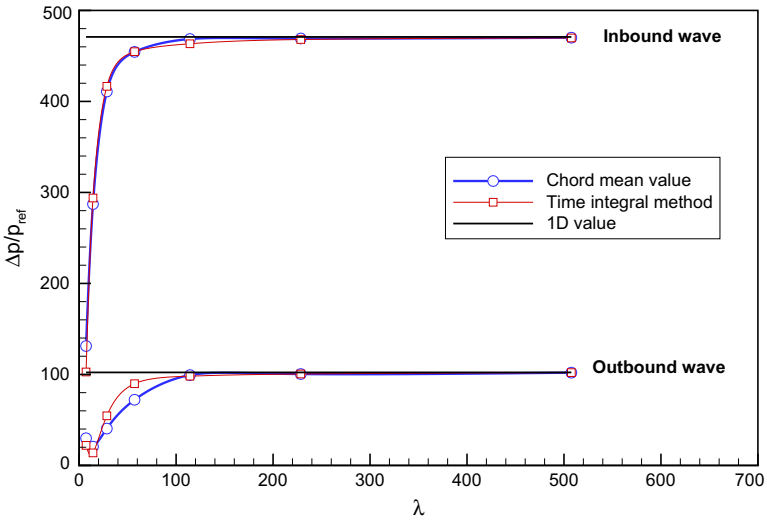

Fig. 8. Mesh sensitivity of the remapping techniques.

one-dimensional method badly. This observation is consistent with Catlin et al. [7]. However, as the frequency is raised, remapped data from both techniques converge to the correct overpressures. To this regard, these techniques are equivalent.

In order to perform the computations for $\lambda = 507$, for instance, the mean chord value technique needs approximately 30 s computer time and less than 1 MB of memory, while the time integral technique needs about 900 s in computer time and up to 100 MB of memory.

Fig. 9 shows the distribution, after data remapping, of the overpressure on a cross-section of the three-dimensional domain. The mesh shown in each sub-figure is an illustration of the mesh corresponding to that particular λ. The time varia-

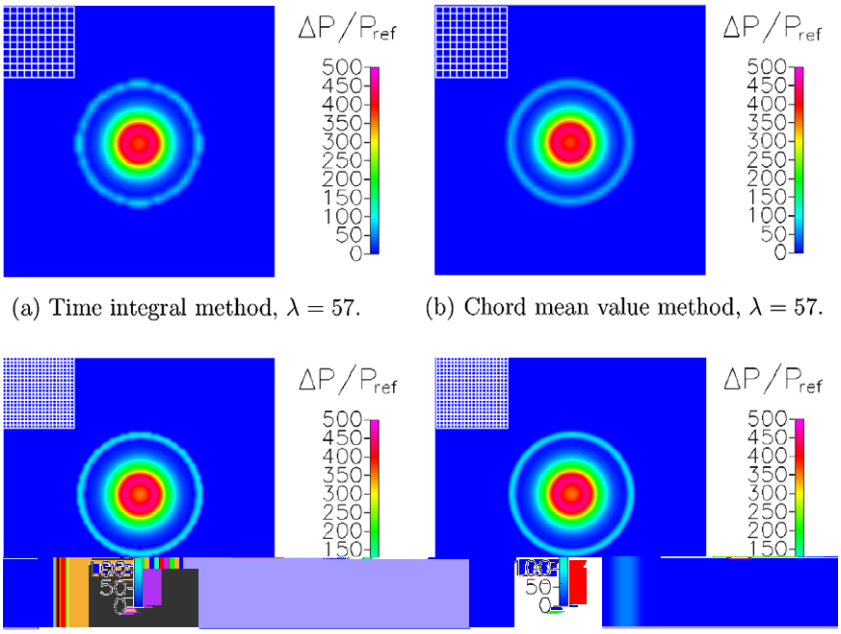

(a) Time integral method, $\lambda = 57$. (b) Chord mean value method, $\lambda = 57$.

iod, $\lambda = 114$. (d) Chord mean value method, $\lambda = 114$. (c) Time integral metl

Fig. 9. Iso-pressure on the middle cross-section.

tions integration method roughly conserves the flow isotropy (cases a and c), while the chord mean value method behaves well considering the isotropy conservation (cases b and d).

Because of its low computer resources consuming and isotropy conservation, the chord mean value technique is chosen to perform the following 1D–3D data remapping.

3.4. Results

Two test cases involving the detonation and the blast wave propagation in complex geometries are performed: a blasting wave inside a closed and rigid box and a blasting wave at the entrance to a tunnel with bifurcation. Calculation results are compared to both numerical and experimental data for the latter case [4].

3.4.1. Case 1

A TNT spherical charge of 1 kg is located at the center of a box of 1 m on each side. The JWL parameters for TNT explosive are summarized in Table 1. The simulation time is 5 ms. The procedure used to perform the simulation is described below.

First, the one-dimensional simulation is performed with a space step $\Delta r = 10^{-4}$ m over a time $T^{1D} = 2 \times 10^{-4}$ s. This time corresponds to a wave propagating up to 0.43 m from the blast center. In the early simulation stage the time step Δt^{1D} is about 2.5×10^{-11} s and increases with time, as mentioned earlier, until about $\Delta t^{1D} = 2 \times 10^{-9}$ s. At this stage, the data are prepared in order to be introduced as initial conditions for the three-dimensional simulation part through the discussed remapping technique. Since the three-dimensional mesh size is approximately 150 times larger than the one-dimensional stencil, the corresponding time step Δt^{3D} is much larger, of the order of 10^{-6} s, at the beginning of the three-dimensional simulation part. For a three-dimensional simulation which proceeds from the blast onset, the time step drops to $3 \times 10^{-10} s$. In other words, for the same mesh size, while the simulation time using the 1D–3D combined method takes about one hour CPU-time, it turns quite prohibitive using the fully three-dimensional approach since it would take considerably much more time. In this regard also, the 1D–3D combined method seems to be highly desirable and more efficient compared to an approach that handles three-dimensional simulation of the blast waves from the onset.

Fig. 10 represents the evolution of the Mach number distribution. Although the mesh is Cartesian, the spatial isotropy is well preserved until blast wave reaches the solid walls where it is reflected and propagates back away from these walls. This leads to complex wave patterns. Because of space propagation, where wave strength decreases as inverse square of the distance, combined with numerical dissipation, the energy of the flow quickly decays [1]. In fact, no significant flow disturbance remains after 0.6 ms and the flow can be considered at rest.

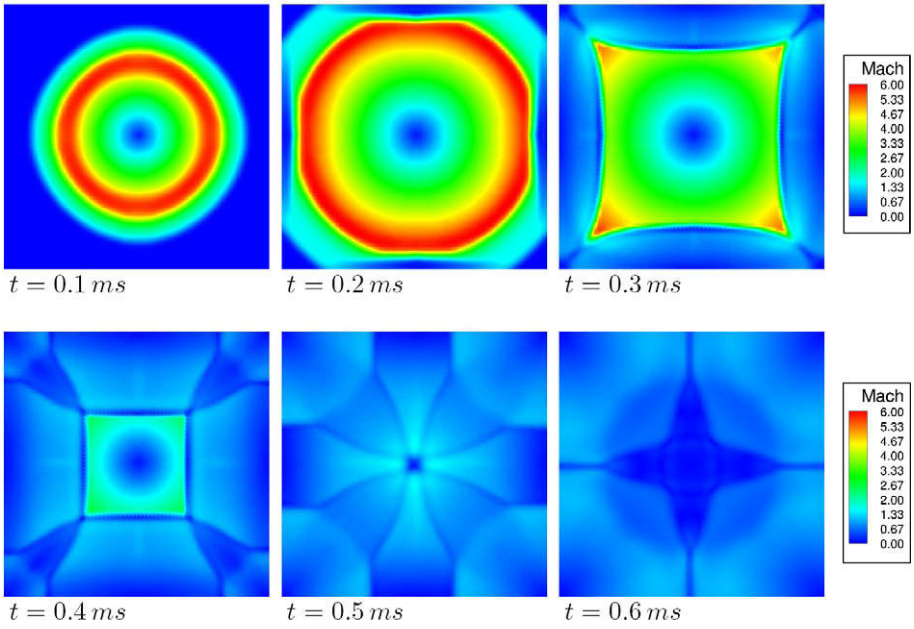

Fig. 10. Distribution of the Mach number at different times.

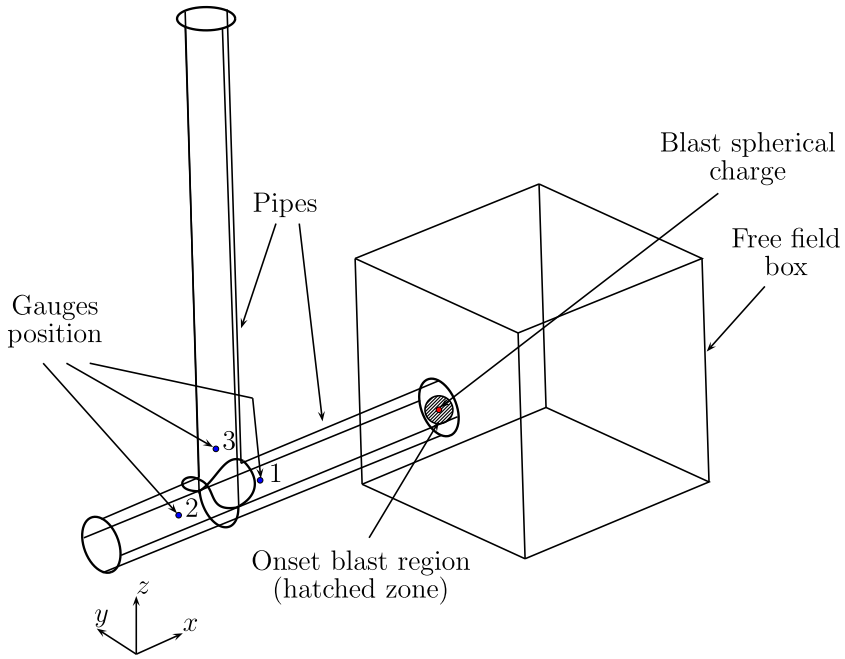

Fig. 11. Three-dimensional tunnel model.

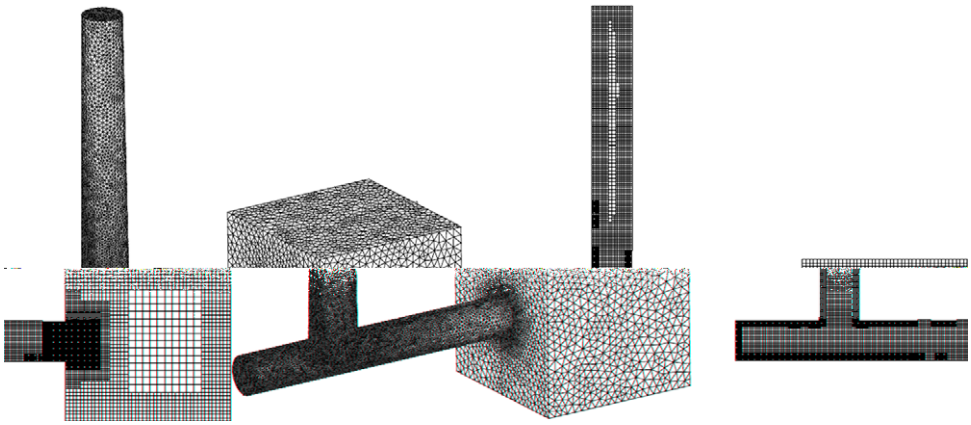

Fig. 12. Illustration of the three-dimensional mesh used to perform the simulation. Left: the surface mesh, right: the mid-spanwise cross-section mesh.

3.4.2. Case 2

The second three-dimensional configuration is a tunnel with bifurcation [4]. Two pipes, of diameter $d = 0.168$ m and length $l = 1.28$ m, are placed orthogonally to each other. The explosive TNT charge, $M_c = 18.5$ g, is located at the entrance of the horizontal pipe. The TNT parameters remain unchanged from above. Two pressure-gauges are placed at the symmetry axis of this pipe before and after the bifurcation. A third gauge is placed at the symmetry axis of the vertical pipe. The details of the configuration are depicted in Fig. 11.

Approximately 2.4 million mesh cells were used. The onset blasting region, see Fig. 12, was more finely meshed ($\lambda = 89$) compared to the far blasting region ($\lambda = 45$). On a 2 GHz AMD® machine, the simulation required about 150 h to perform 5 ms simulation time.

Figs. 13–15 represent the overpressure history recorded at gauges 1, 2 and 3, respectively, obtained from the current simulation. Corresponding experimental and other numerical data from Rigas et al. [4] are also shown in the same plots. Although some delay can be mentioned, less than 0.1 ms, the current simulation results noticeably fit well with the experimental data. The discrepancy is less than 15% which is quite consistent with the information loss recorded when remapping data at $\lambda = 89$ as shown in Fig. 8. For gauge 1, the first peak, where the overpressure reaches about 20 Bars,

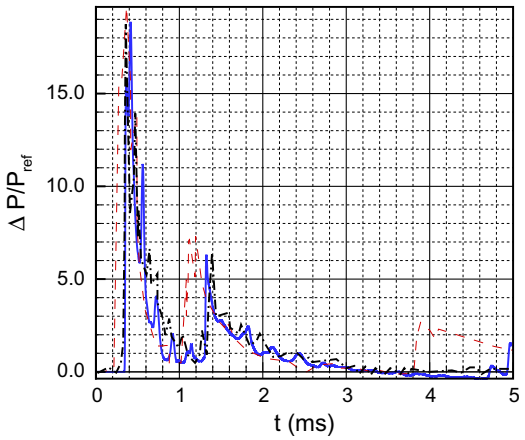

Fig. 13. History of the overpressure at gauge 1.

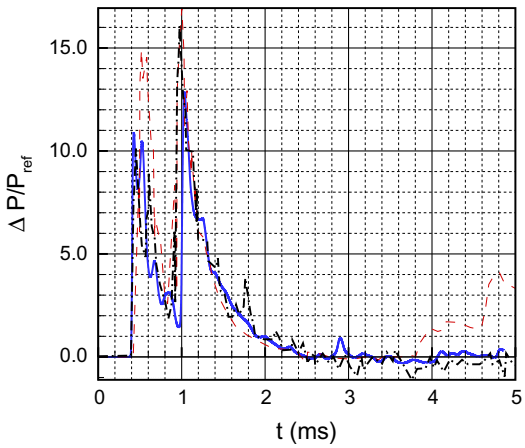

Fig. 14. History of the overpressure at gauge 2.

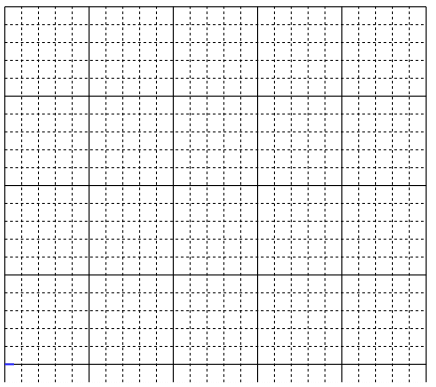

corresponds to the Mach reflection shock wave on the wall of the horizontal pipe. The second peak, which comes very close to the previous one, corresponds to the incident wave that comes from the blast charge. This wave is slower than

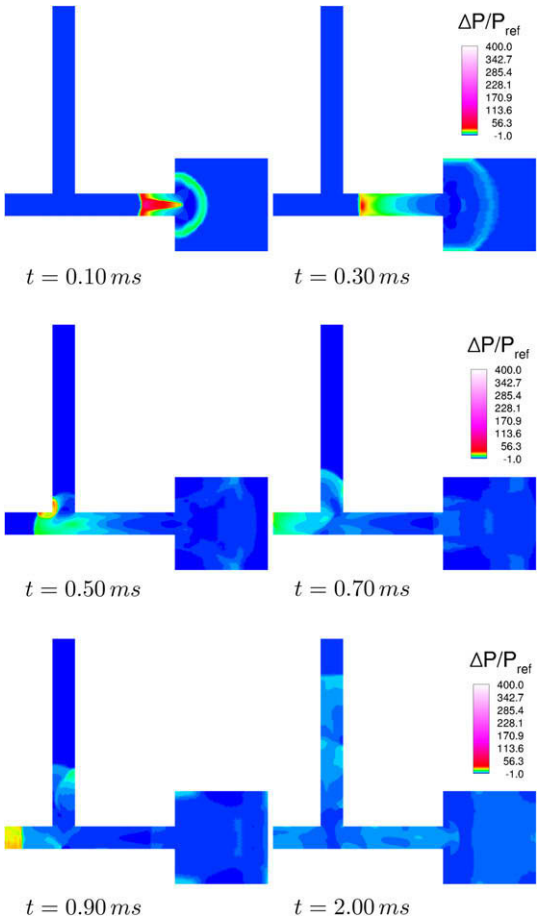

Fig. 16. Distribution of the overpressure at different simulation times.

the Mach shock wave [6]. The third peak corresponds to the second incident wave from the blast center as discussed in Section 2.2. The following – much weaker – peak corresponds to the reflected wave at the closed end of the horizontal pipe. The pressure tends rapidly, in about 3 ms, toward the initial pressure. Concerning gauge 2, the first three peaks are the same as for gauge 1, but the overpressure is about 50% less because of the influence of the branch. The forth main peak, which is higher than the first, is due to the superposition of the decaying incident waves and the reflected wave at the end of the horizontal pipe. Pressure signature at gauge 3 is similar as at gauge 1 with weaker overpressure, however. The relevant plot shows two first peaks due to the Mach shock and incident blasting wave, while the following main one is due to reflected waves at the end of the horizontal pipe. Although not recorded by the experiments, the last peak, at about 4.5 ms, is the reflected wave at the end of the vertical pipe. Lateral reflections on the vertical pipe are extremely weak to be distinguished on gauge 3.

Figs. 16 and 17 show the distribution of the overpressure and the Mach number, respectively, over the tunnel for several times until the disturbance attains the end of both pipes. As can be expected, the detonation produces a violent pressure rise followed by a rapid gas expansion in both sides of the blast charge. However, the overpressure quickly diminishes in the – right – free region and hence hot gases are highly accelerated as can be shown in Fig. 17, although the front wave becomes subsonic a short time after the detonation ($t < 0.1$ ms). Hence in this region, no shock wave occurs at a relatively small distance of the blast center. It is worthwhile to also notice that the flow expansion right the blast charge and the pressure decaying inside the pipe induce a quasi-steady flow in the free region. The long persistence of the mushroom-shape of the Mach distribution in this region is moreover a manifestation of that. In addition, since the left side of the blast charge is a confined region, the overpressure across the wave front is maintained high over a much longer distance inside the horizontal pipe than in the free region. The wave is supersonic even through and after the branch. Still, as mentioned above, the overpressure drops down at the branch particularly inside the vertical pipe. This may be beneficial in two ways. In one hand, the presence of the vertical pipe significantly cuts the overpressure inside the horizontal pipe, and hence reduces the wave strength behind the branch. In the other hand, the part of the wave propagating inside the vertical pipe becomes transonic shortly beyond the

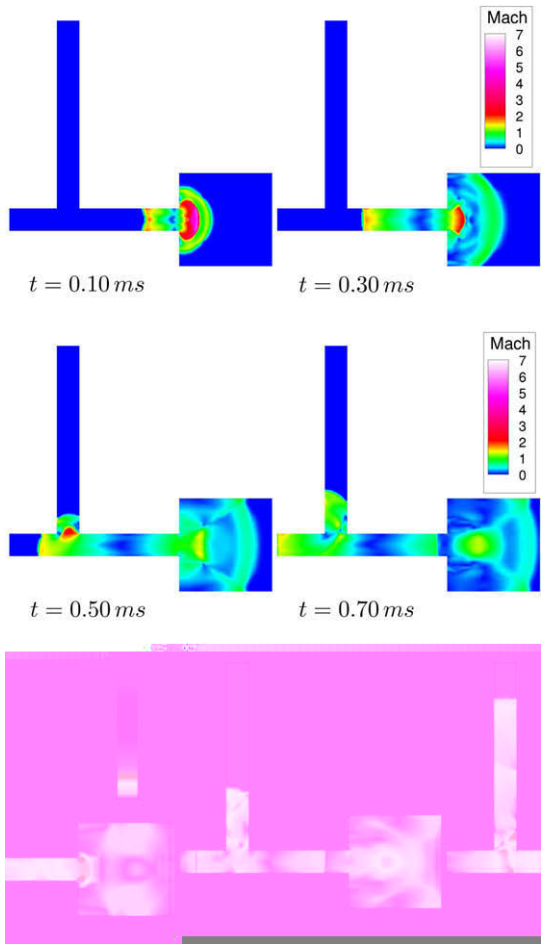

Fig. 17. Distribution of the Mach number at different simulation times.

branch. Since no shock occurs in subsonic regime, this wave is not so important and dangerous than the one propagating inside the horizontal pipe. The bifurcation device inside confined domains may be interesting from a safety point of view.

4. Conclusion

The blast wave generated by a detonating charge is modeled and simulated in two parts. The first part is performed, where the flow isotropy is satisfied, by a one-dimensional radial model. Both perfect gas and Jones–Wilkins–Lee laws governing hot detonation products are examined. Strong shock traveling through the fluid flow is successfully captured by the numerical model. In one hand, perfect gas law leads to slightly overestimating the maximum peak of pressure while JWL law gives, at lower numerical cost than the perfect gas law, high quality results compared to both experiments and numerical data found in the literature. In other hand, the arrival time is under-estimated when considering perfect gas law, while JWL law correctly estimates it.

Among the tested 1D–3D remapping techniques, the chord mean value method is found to satisfy best at the same time accuracy, robustness and low computing cost criteria. This technique has therefore been used to supply with initial conditions the three-dimensional simulation part.

The one-dimensional part, the remapping technique and the three-dimensional part constitute the proposed 1D–3D combined simulation method.

Two three-dimensional simulations are performed. The first case is a rigid and closed box configuration inside which an explosive charge detonates. Simulation is performed and some blast wave patterns are depicted. Especially, wave reflections on the walls and interference in the bulk were clearly distinguishable. The second performed case is the blast wave simulation inside a tunnel with bifurcation. The comparison between experimental data and the simulation results shows good agreement. It is found that in confined domains, the flow remains supersonic a long distance from the blast charge. The bifur-

cation leads to reducing the overpressure inside the main pipe while the overpressure inside the secondary pipe is weaker and the flow is transonic. In confined structures, this suggests the effectiveness of such measures in order to be a safety emergency space.

Improvement of the presented numerical model are under development by considering adaptive mesh refinement in order to describe more accurately and less costly the blasting wave front and the subsequent interactions with structures.

Acknowledgments

The authors wish to acknowledge D. Uystepruyst for his helpful and fruitful suggestions about various numerical issues. This work is carried out in the EGSISTES project supported by the French National Research Agency, ANR under contract R287.

References

[1] H.L. Brode, Numerical solutions of spherical blast waves, Journal of Applied Physics 26 (6) (1955) 766–775.
[2] J.M. Dewey, The air velocity in blast waves from T.N.T. explosion, Proceedings of the Royal Society of London A121 (1964) 366–385.
[3] W.E. Baker, P.A. Cox, P.S. Westine, J.J. Kulesz, R.A. Strehlow, Explosion Hazards and Evaluation. Fundamental Studies in Engineering, Elsevier, New York, 1983.
[4] F. Rigas, S. Sklavounos, Experimentally validated 3-D simulation of shock waves generated by dense explosives in confined complex geometries, Journal of Hazardous Materials A121 (2005) 23–30.
[5] S. Sklavounos, F. Rigas, Computer simulation of shock waves transmission in obstructed terrains, Journal of Loss Prevention in the Process Industries 17 (2004) 407–417.
[6] S. Trélat, Impact de fortes explosions sur les bâtiments représentatifs d'une installation industrielle, Ph.D. Thesis, University of Orléans, France, 2006.
[7] C. Catlin, M. Ivings, S. Myatt, D. Ingram, D. Causon, L. Qian, Explosion hazard assessment: a study of the feasibility and benefits of extending current HSE methodology to take account of blast sheltering, Sheffied Health and Safety Laboratory, Report No. HSL/2001/04, 2001.
[8] C.A. Mills,The design of concrete structures to resist explosions and weapons effects, in: Proceedings of the First International Conference for Hazard Protection, Edinburgh, 1987.
[9] J.M. Henrych, The Dynamics of Explosion and its Use, Elsevier, Amsterdam, 1979.
[10] H.L. Brode, Blast waves from a spherical charge, Physics of Fluids 2 (2) (1959) 217–229.
[11] C.L. Mader, Numerical modeling of explosives and propellants, second ed., Journal of Hazardous Materials, University of California, Berkeley, 1998.
[12] R.C. Johnson, Calculations of real-gas effects in flow through critical-flow nozzles, Journal of Basic Engineering (1964).
[13] A.B. Kaplun, A.B. Meshalkin, On the structure of a general equation of state for liquid and gases, Doclady Physics 46 (2) (2001) 92–96.
[14] E. Lee, M. Finger, W. Collins,"JWL equation of state coefficients for high explosives", Lawrence Livermore Laboratory Report, UCID–16189, 1973.
[15] S. Itoh, H. Hamashima, K. Murata, Y. Kato, Determination of JWL parameters from underwater explosion test, Science, Technology and Energy Matter 64 (2003) 248–253.
[16] R. Peyret, T.D. Taylor, Computational Methods for Fluid Dynamics, Springer-Verlag, New York, 1983.
[17] J.P. Boris, D.L. Book, Flux-corrected transport. I. SHASTA, a fluid transport algorithm that works, Journal of Computational Physics 11 (1) (1973) 38–69.
[18] F. Waymel, F. Monnoyer, M.J.-P. William-Louis, Numerical simulation of the unsteady three-dimensional flow in confined domains crossed by moving bodies, Computers and fluids 35 (2005) 525–543.
[19] F. Deister, F. Waymel, E.H. Hirschel, F. Monnoyer, Self-organizing hybrid cartesian grid generation and application to external and internal flows, Numerical flow simulation III, Notes on numerical fluid mechanics and multidisciplinary design 82 (2002) 18–29.
[20] B. van Leer, Towards the ultimate conservative scheme, V. A second-order sequel to Godunov's method, Journal of Computational Physics 32 (1) (1979) 101–136.